,

Enhancing the Resilience of Energy Systems: Optimal Deployment of Wave Energy Devices following Coastal Storms

Umesh A. Korde[1, a)]

Dept. of Environmental Health and Engineering, Johns Hopkins University, Baltimore, MD 21218.

(Dated: 11 July 2020)

Isolated coastal areas and remote islands may be particularly vulnerable to damage from powerful storms, storm surges and flooding. Because wave energy converters are designed to survive rough seas and can be transported by sea, they could potentially play a role in post-storm operations and contribute to power-grid recovery. To that end, this paper addresses questions such as how many devices would need to be deployed and in what sequence, in order to optimize some performance index that includes, as functions of time, both, the energy needed, and the energy converted by the device units.

In this work, the wave-by-wave dynamics of the devices are controlled to optimize mean power conversion over 20 minutes, assuming sea-state stationarity over that period. Sea-state variations between 20 minutes and 13 hours are found to be small (relative to variations between 13–60 hours) for a candidate deployment site near a Caribbean island. Targeting deployment over 5–7 days, two optimization schemes are considered: (i) maximization of the power conversion capacity over a specified time interval, and (ii) minimization of the time taken to deploy the desired conversion capacity. With the wave energy devices controlled for optimal conversion over successive 20-minute periods, the optimization is carried out over the number of converter units added as a function of time.

Results indicate that optimal deployment sequences can be evaluated for given conversion capacity/recovery-time targets and the type of recovery desired [strategies (i) or (ii) above]. However, depending on the energy richness of the 'normal' wave climate at the deployment site, cost-effective recovery may require closer consideration of the trade offs among device configurations, size, and number of units needed for desired capacity. The potential for wave energy devices to power early recovery operations and to support power-grid black-start could be worth considering further as a means to enhance the resilience of coastal and island energy systems.

[a)]Electronic mail: ukorde1@jhu.edu.

NOMENCLATURE

$\eta(x;t)$ Wave-surface elevation at point x and time t.

ω Angular frequency variable for incoming wave input.

$\overline{a}_r(\infty)$ Infinite-frequency added mass in heave.

Ψ_D, Ψ_R Performance index for determining required-power function; converted-power function.

τ Time variable for deployment; in hours.

φ Angular parameter used to solve for G and R under minimum time deployment strategy.

ζ Dummy variable for time integration leading to actuator/control force.

a Acceleration-like parameter used in the minimum-time strategy.

$a_r(\omega)$ Fourier transformable part of the frequency-dependent added mass at ω; $a_r(\omega) = \overline{a}_r(\omega) - \overline{a}_r(\infty)$

$b_r(\omega)$ Radiation damping due to device oscillations at frequency ω

c_d Linearized viscous-friction damping.

D The difference between the targeted $G = G_R$ and demand currently being served.

F_{cr} Control/actuation force applied by power take-off.

G Required power function (i.e. power required for recovery applications).

h_c Impulse-response function to be synthesized to enable real-time wave-by-wave control.

h_l Impulse response function representing the wave propagation model.

h_r Radiation impulse response function.

H_s Significant wave height.

H_{sm} Monthly mean significant wave height.

k Stiffness coefficient opposing oscillation (hydrostatic for heave, pitch, etc.

m In-air mass of the oscillating element of the device.

P_s, P_c, ℓ 20-minute average converted power, 20-minute average incident wave power, and conversion efficiency, resp.

R Function representing wave-generated power as units are added.

R_0 Wave power conversion function (of τ) for monthly mean wave statistics.

R_n Change in wave power conversion due to nth significant spectral variation.

S Power spectrum.

t Time variable for device dynamics; in seconds.

T_e Energy period.

T_{em} Monthly mean energy period.

U Number of device units.

u Velocity of device oscillating element.

x_A Point of up-wave wave profile measurement.

x_B Device centroid location.

$\mathscr{L}$ 'Lagrangian' defining the integrand for the functional representing performance index.

I. INTRODUCTION

Recently documented work indicates that the impacts of climate change could be serious for coastal communities[1,2]. In particular, as a consequence of rising sea levels, coastal storms could become more frequent and more intense, and more likely to precipitate storm surges and floods[1]. Recent examples of highly destructive storms that affected the Caribbean region and the east coast of the United States include Hurricane *Maria*[3] and Hurricane *Michael*[4]. Acute coastal events may often take a heavier toll on isolated coastal regions and islands[5]. Power grids in some regions may be particularly vulnerable due to isolation from the nearest functioning macrogrids, and power restoration may require 'external' power sources such as diesel generators or batteries that may

be hard to transport in case of widespread infrastructure damage[5]. In such situations, energy converters that are designed to withstand rough seas and can be transported by sea could provide a plausible option worth evaluating further. As coastal storms continue to grow more frequent and more intense[2], so would the need for additional external power sources. To that end, it might seem increasingly worthwhile to investigate the potential to use floating-body wave energy converters[6,7] to assist in overall recovery operations and grid restart. As a step in that direction, this paper explores whether there might be an optimum strategy to derive the most benefit from successively deployed wave energy devices, and whether any intrinsic limits exist, on the capacity of a class of present day devices to meet the necessary power demands.

While attempts to use wave energy have been reported since the late 18th century[8], serious efforts to utilize ocean waves for large scale energy generation began with the work of Salter[6]. Efficient power conversion in energy-rich swells required large devices, posing serious design challenges[9,10]. Smaller devices such as heaving axisymmetric buoys utilizing favorable 3-dimensional interactions with incoming waves also began to be developed in the 1970's[11]. These devices could respond equally to surface waves incident from any direction ('omni-directional devices'). While the Salter duck and Evans cylinder devices received incoming waves 'broad-side on' (i.e. in the beam-sea configuration), other devices were also developed in the 70's that performed in the 'head-sea' configuration, and were shaped more like ships[6,12,13].

More recent examples of head-sea devices include the Pelamis system that extends the oscillating 'spine' with hydraulic actuators as originally developed for use with the Salter duck[14]. Recently tested devices also include the floating Wave Dragon[15], which extends the shallow-water TAPCHAN system developed in the late seventies[16]. This device uses wave-overtopping into a reservoir to drive a turbine. Of the three types of devices, the head-sea and omni-directional devices are likely more efficient structurally[17]. It is interesting to consider that the *Kaimei*, one of the earliest wave energy devices to be ocean-deployed[13], was essentially a ship modified to create 22 oscillating water column chambers open at the bottom. It is likely that devices such as the *Kaimei* may prove to be of interest to the objectives of this work. However, for convenience, an axisymmetric buoy type device with the geometry described in[18] is used in this paper. It should be pointed out that this device can be 'self-contained', which could facilitate deployment.

This work assumes that the devices to be deployed are controlled for maximum efficiency, so that the smallest practical number of units may be used to meet given recovery needs. Active control of the hydrodynamic response provides one way to enhance annual energy conversion with

small devices, thereby increasing the overall likelihood of cost-effective operation[10]. Indeed, efforts to increase response bandwidth by controlling the phase of the force applied by the power take-off were first reported in the seventies[11,19]. For the Salter duck, control was accomplished by including a reactive component in addition to the resistive part in the torque opposing the duck oscillation, and by independently adjusting the magnitudes of the two parts. Investigations on small heaving point-absorber devices with short resonant periods led to the development of the 'latching' concept[20], though this is not the type of control used in this work. Work on single-mode reactive control led to multiple-mode impedance matching approaches termed 'complex-conjugate control'[21,22], which could be applied in the frequency-domain for peak-frequency tuning in changing wave spectra. At-sea tests on reactive + resistive loading were performed a few years ago on prototypes of the Wave Star device[23], and a 2-3 fold improvement in annual power production was reported. Application of reactive and resistive loads to produce correct impedance matching conditions on a wave-by-wave basis in irregular waves presents a fundamental challenge. As has been known since the mid-eighties, wave-by-wave control of a wave energy converter for maximum power conversion requires knowledge or prediction of the incoming wave field[24,25]. In particular, prediction or foreknowledge of the wave elevation is needed for about 20-30 s into the future (i.e. as far forward into the future as the causal impulse response function for the device has memory into the past). Wave predictions based on a deterministic propagation model were used to approximate wave-by-wave impedance matching control in computer-generated wave records, and in simulations significant improvement in capture width ratio was observed for a 2-body heaving axisymmetric device having the same geometry as that used in the present paper[26]. Consistent with the practice in the wave energy literature, the wave input was assumed to be stationary over a 20-30 minute period[27], so that wave spectra and wave statistics such as the significant wave height H_s and energy period T_e could be assumed to hold steady over that time period.

Wave energy devices vary widely, but some configurations (ship forms, some types of buoys, etc.) may be a natural option to consider for power restoration following a coastal disaster, since they can be towed over to the site and slack-moored in place. Since such devices might need to operate in shallower waters, shallow-draft buoys rather than spar-type buoys may be preferred when the buoy-type devices are to be used. Transportability by sea would minimize the dependence on road transportation and other land-based infrastructure, and the devices could perhaps be connected to an accessible temporary power hub on the shore without much difficulty. In the long run, some prior pre-storm-season preparation such as erection of temporary water-front power hubs at

vulnerable coastal sites may be desirable. The time taken to establish a firm connection to the shore hub needs to be considered further, but is not included in the present treatment of Section II. From this standpoint, larger ship-forms encompassing a number of small converter units (such as the *Kaimei*) may be preferable, as they would likely require only a single shore-connection (as opposed to several, as in the case of buoys). The possibility of wave energy devices being deployed for energy resilience and recovery following an extreme coastal event was discussed recently in a U.S. Department of Energy (DOE) report (referenced earlier in this introduction), under the backdrop of the current recovery practices employed by the US Federal Emergency Management Agency (FEMA)[5]. Effects of extreme coastal events can include damage to portions of the local power grid, temporary incapacitation of the power generation facility supporting the affected area, or both. Power grid recovery frequently involves drawing power from other connected regions to help the local grid restart itself[28], except when the nearest possible sources also experience outage[29]. For island grids and coastal grids serving isolated areas, nearest external sources of power may be inaccessible, and the local grid then faces the 'black-start' situation. Diesel generators transported to the affected site are frequently used as external power sources (examples include FEMA's diesel generators, ranging from 1.5 kW to 1.8 MW[30]). Other power sources such as fuel cells, solar and wind energy converters have been considered for isolated grids[31]. Large-capacity batteries have also been used (e.g. at power capacities as high as 5 MW and 33 MW[32]). While small, distributed microgrids based on renewable energy sources with supporting batteries may be preferred in a number of situations[33], they are at present less common than larger macrogrids[5]. In some coastal regions and islands, there may be an over-dependence on a single, often wholly imported power source. A related example is that of a part of the coast of Oregon, where a bulk of the power is transmitted across a mountain range[34], which results in a local grid that is 'fragile'. In addition, diesel generators and batteries may be hard to transport by land, depending on the extent of damage; and could even pose additional environmental risks. It therefore appears worth considering wave energy devices as a potential source of power to aid in grid black-start and to support short-term emergency recovery operations.

In the work discussed in this paper, the wave-by-wave dynamics of the devices are controlled to optimize mean power conversion over successive 20-minute periods, assuming sea-state stationarity over that duration. Sea-state variations between 20 minutes and 13 hours are also found to be small (relative to variations between 13-60 hours) for the wave climate at the proposed deployment site. It is supposed that the wave energy devices are delivered by sea in small numbers, and are

deployed (i.e., set up, and connected for power delivery) in a phased manner. 'Power conversion capacity' here is defined as the maximum power that can be converted, as determined by the number of devices deployed (each operating under constrained wave-by-wave impedance-matching control). Targeting deployment over 5-7 days, two optimization schemes are considered: (i) maximization of the power conversion capacity over a specified time interval, and (ii) minimization of the time taken to deploy the desired conversion capacity. With the wave energy devices controlled for optimal conversion over each successive 20-minute period, the optimization can be carried out over the number of converter units added as a function of time, if the units are arranged so as to avoid interactions (positive or negative). It should be noted that only the energy conversion aspect is included in the present optimization scheme, and costs are not included.

Section II following this introduction discusses the overall formulation used in the present work. Section III summarizes the calculations performed and the results included here. The results are discussed in IV. The paper concludes with V, which outlines the principal conclusions of this work.

II. FORMULATION

This section describes the overall methodology used here to determine optimal deployment sequences for wave energy device units following a storm-caused large scale power outage. It is not practical to deploy all of the required units at one time. However, recovery operations require that power conversion and delivery begin at the earliest. It should be pointed out that resilience is frequently defined as the area under the 'resilience triangle' where linear recovery is assumed[35]. In the present context, this would translate into a sudden drop in power capacity following an extreme event such as a coastal storm/hurricane, and a more gradual recovery over a length of time. The present paper investigates whether and how different the optimum recovery path may be from a straight line, and considers a variational optimization technique to derive optimal recovery trajectories. It is recognized that the optimum trajectory may be dependent on the definition of the performance index and the optimization criterion selected. Two straightforward implementations are considered here. The approach in (1) below is referred to as the 'maximum capacity deployment over specified time period', while the approach in (2) represents the minimum time deployment. The goals of the two strategies are summarized below.

1. To find a function of time that maximizes the power demand served over a prescribed length

of time. Then, to evaluate a function of time that describes the desired temporal evolution of the power conversion capacity,

2. To evaluate the temporal evolution of the power demand and the power conversion functions simultaneously, so that a prescribed level of conversion capacity is reached in the shortest time.

A measure of resilience is thus arrived at here (1) as maximum power recovered over a prescribed duration, and in (2) as the time taken to recover specified power capacity. It is important to recognize first that the two strategies are to be employed in an environment where the incoming energy is subject to changes on multiple time scales. Thus, wave profiles vary incessantly, on time scales of 1–20 seconds. Wave statistics, on the other hand, (i.e. power spectral density $S(\omega)$, significant wave height H_s, energy period T_e, etc.) remain valid for 20-30 minutes[27]. In general, H_s, T_e may vary over time scales of 2–12 hours depending on the wind-sea/swell contributions, while variations on longer time scales occur over larger spatial scales and with seasonal changes. Deployment off the coast of Puerto Rico is considered in this work, where wave measurements are available off Rincon, from a wave data buoy at the CDIP station 181[36].

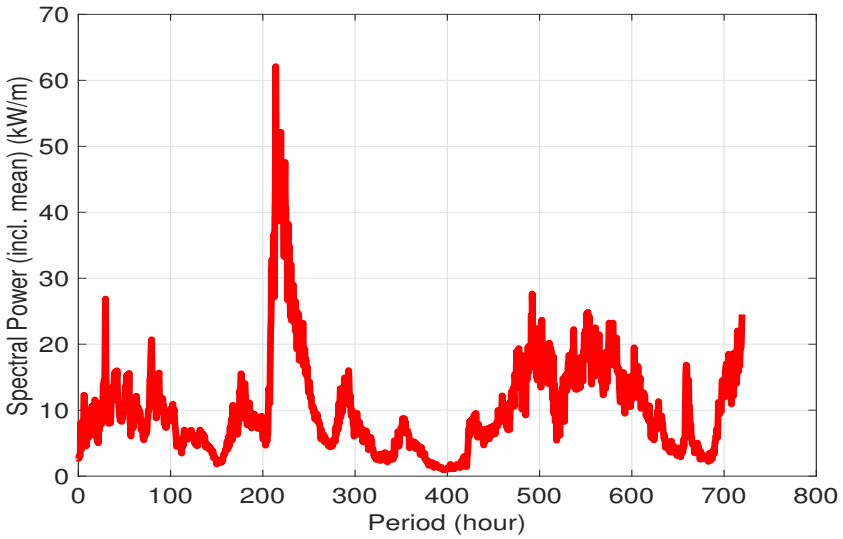

FIG. 1. Spectral density variation over 1-month: UCSD CDIP station 181; Rincon, Puerto Rico; November 2016; monthly mean conditions: $H_{sm} = 1.4$m, $T_{em} = 9.4$s.

Figure 1 shows the wave spectral density variations based on the CDIP 181 data, while Figure 2 shows the variations about the monthly mean statistics that are relevant to the deployment period

(i.e. in magnitude and period).

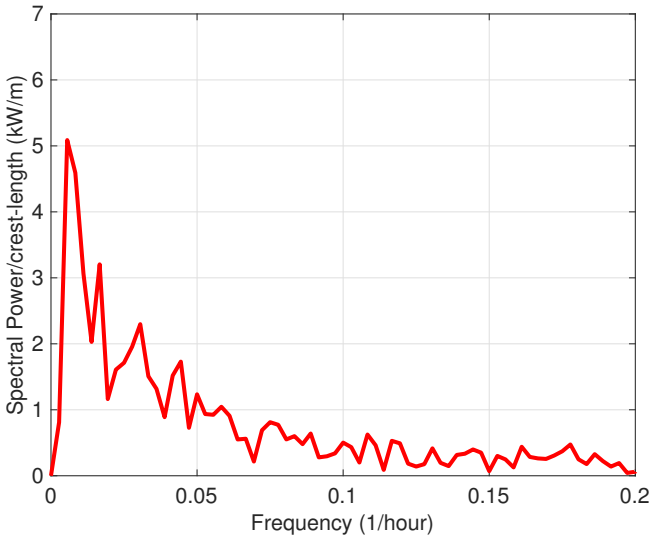

(a) Spectral Density Variations (frequency)

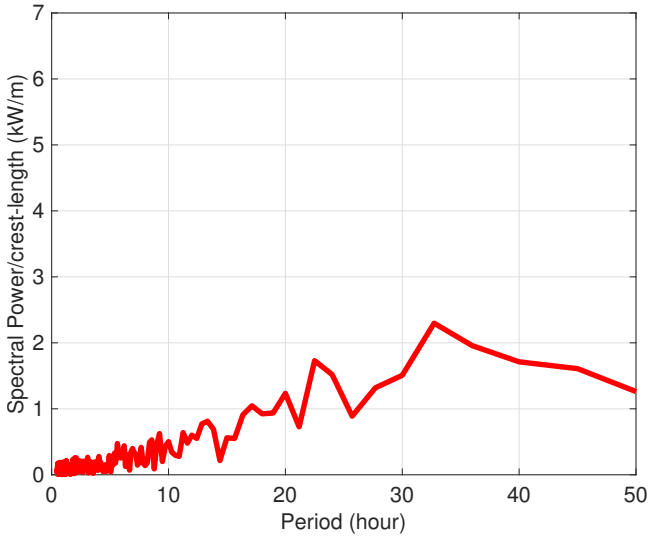

(b) Spectral Density Variations (time)

FIG. 2. Spectral density variations about the mean, showing that 4 periods: 13 hours, 23 hours, 33 hours, 60 hours have energy density variations large enough to influence performance over a 5-7 day period.

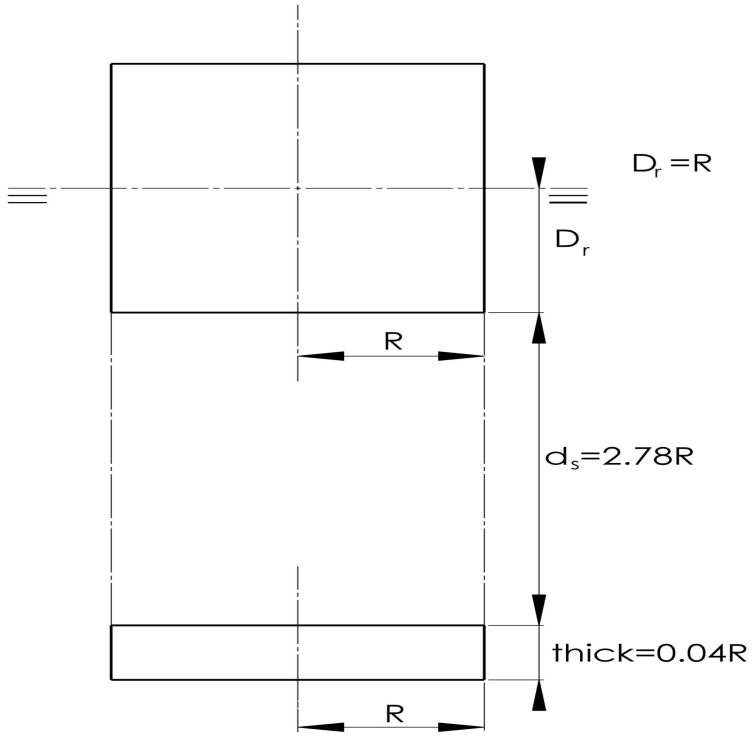

FIG. 3. The heaving axisymmetric device used in this work. Relative oscillation is utilized for energy conversion with a hydraulic cylinder type power take-off mechanism/actuator. The power take-off also applies the required control force in this work. The dimensions are based on the configuration studied in[18].

The wave-statistic variations are addressed in the manner described later in this section. The wave energy device used in this study is a 2-body axisymmetric system, with the relative heave oscillation being used for power conversion. The power take-off system is assumed to be electro-hydraulic. The device used here is a geometrically scaled version of the system considered in this author's previous work[26,37] (see Figure 3 for a schematic view of the system). It should be noted that the treatment below assumes that the incident waves and the device response both are linear. Near-shore waves may not be strictly linear, however, in which case, the treatment below will be valid to first-order. Since both force and velocity below will likely miss second-order effects, the uncertainty in estimates of power generation below needs further attention. Further, even though a moderately large number of buoy units are expected to be deployed, interaction effects[38], whether positive, or negative are here neglected. However, this aspect would need to be considered, perhaps, in the form of a constraint on the number of units to be deployed over a given area.

As shown by Falnes[39], the relative oscillation behavior can be expressed using an equivalent 1-degree of freedom system. This equivalence is discussed further in other references[26,40].

Device dynamics for single-mode oscillation in real time need to be described with an integro-differential equation[41],

$$[m+\bar{a}_r(\infty)]\dot{u}(t)+\int_0^\infty h_r(\tau)u(t-\tau)d\tau+c_d u(t)+k\int_{-\infty}^t u(\tau)d\tau=F_f(t), \tag{1}$$

where, m, $\bar{a}_r(\infty)$, c_d, and k denote, respectively, the in-air mass, infinite-frequency added mass, linearized viscous friction damping, and hydrostatic stiffness of the oscillating element of the device, u is the oscillation velocity, and h_r is the radiation impulse-response function. $h_r(t)$ must be *causal* ($h_r(t)=0, t<0$), hence, the real and imaginary parts of its Fourier transform satisfy Kramers-Kronig relations[42]. Alternatively,

$$h_r(t)=\frac{2}{\pi}\int_0^\infty b_r(\omega)\cos\omega t d\omega=-\frac{2}{\pi}\int_0^\infty \omega a_r(\omega)\sin\omega t d\omega, \tag{2}$$

where $a_r(\omega)$ denotes the frequency-variable added mass function (i.e. excluding the infinite-frequency added mass), and $b_r(\omega)$ represents the frequency-dependent radiation damping. Because of the constraint (2), a part of the control/actuation force for wave-by-wave 'impedance match' must be *anticausal*[24].

$$F_{cr}(t)=\int_{-\infty}^\infty h_c(\zeta)\eta(x_B,t-\zeta)d\zeta. \tag{3}$$

That is, $h_c(t)=0, t>0$. Therefore, $F_{cr}(t)$ needs to be synthesized using wave-elevation prediction (20–30s ahead). $h_c(t)$ may more conveniently be represented using an odd function $h_a(t)$ and an even function $h_b(t)$, as shown in the Appendix, which also summarizes the dynamic model for the system used in the present work. Additional 'constraint damping' to keep device excursions within practical limits is also needed[38], but not shown in Equation (1). Figure 4 shows the converted power time series for the monthly mean wave conditions ($H_{sm}=1.4$m, $T_{em}=9.4$s).

A. Maximum Capacity Deployment over Specified Time

It is recalled that a measure of resilience is here obtained as the ability of a coastal area to recover maximum power conversion capacity over a specified time interval. As a first step, a function $G(\tau)\geq 0$ is defined that optimizes power demand served over a prescribed time period; here, 5 days, with τ in hours. Next, a wave energy conversion rate function $R(\tau)$ is found that

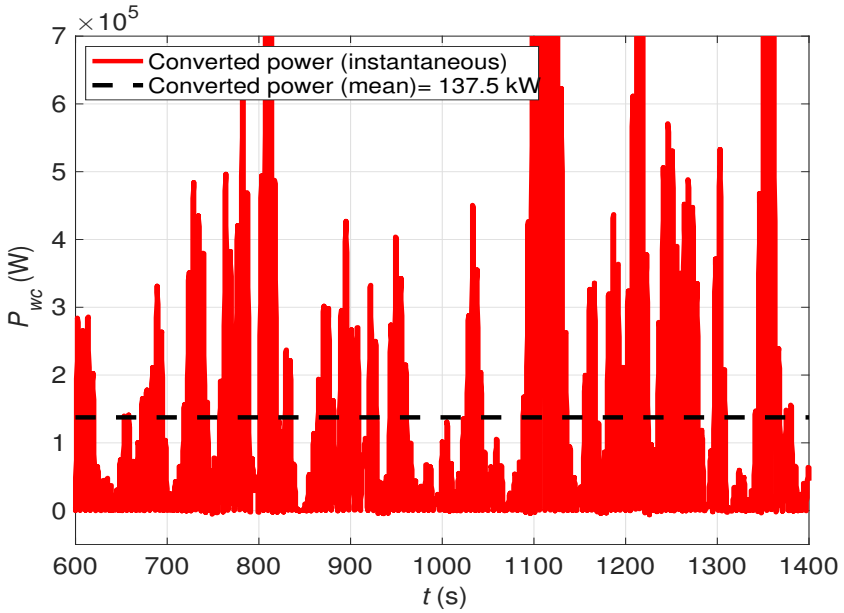

FIG. 4. Converted power time series for the monthly mean wave conditions; $H_{sm} = 1.4$m, $T_{em} = 9.4$s. The plot also shows the mean converted power over 20 minutes.

best matches $G(\tau)$ despite variations in the incident wave conditions. Letting G_R denote the target demand rate to be reached at $\tau = \tau_R$ as G_R (starting from $G = 0$ at $\tau = 0$), the instantaneous difference $G_R - G$ can be defined as,

$$D(\tau) = G_R - G(\tau). \tag{4}$$

The 'action' functional for the function D is defined as Ψ_D[43], where,

$$\Psi_D = \int_{\tau_0}^{T\,\tau_R} \left[(D(\tau))^2 + (\tau_R - \tau_0)^2 \dot{D}^2(\tau) \right] d\tau, \; \dot{D} \equiv dD/d\tau. \tag{5}$$

The goal is to evaluate $D(\tau)$ such that Ψ_D is minimized when its first variation $\delta\Psi_D = 0$. For prescribed τ_0 and τ_R,

$$\delta\Psi_D = \int_{\tau_0}^{\tau_R} \delta\mathscr{L}(D,\dot{D}) d\tau = 0, \tag{6}$$

where $\mathscr{L}(D,\dot{D})$ represents the integrand in equation (5). Equation (6) implies,

$$\frac{\partial\mathscr{L}}{\partial D} - \frac{d}{d\tau}\left(\frac{\partial\mathscr{L}}{\partial\dot{D}}\right) = 0, \tag{7}$$

subject to $D(\tau_0) = G_R$, since $G(\tau_0) = 0$, and $D(\tau_R) = 0$, since $G(\tau_R) = G_R$. G_R is the desired power level to be supplied to the affected region at $\tau = \tau_R$. For example, here, 2 MW, 10 MW,

etc., at $\tau_R = 120$ hours. For $\mathscr{L}$ in equation (5),

$$\frac{d^2D}{d\tau^2} - \frac{D}{(\tau_R - \tau_0)^2} = 0, \tag{8}$$

which leads to the solution, for $\tau_0 = 0$,

$$D(\tau) = G_R \left(\cosh\left(\frac{\tau}{\tau_R}\right) - \coth 1 \sinh\left(\frac{\tau}{\tau_R}\right) \right). \tag{9}$$

With $D(\tau)$ defined as in equation (4), equation (9) leads to,

$$G(\tau) = G_R \left[1 - \cosh\left(\frac{\tau}{\tau_R}\right) + \coth 1 \sinh\left(\frac{\tau}{\tau_R}\right) \right]. \tag{10}$$

To account for the variation in wave spectra, $R(\tau)$ is defined as,

$$R(\tau) = R_0(\tau) + \sum_{n=1}^{N} R_n(\tau), \tag{11}$$

where $R_0(\tau)$ denotes the power conversion rate for the monthly mean spectral conditions, $H_{sm} =$ 1.4m, $T_{em} = 9.4$s, and $R_n(\tau)$ denotes the differences in conversion due to spectral variations about the mean. $N = 4$ here, for the 4 periods (13 hours, 23 hours, 33 hours, 60 hours) identified in Section II. Under constrained wave-by-wave control, conversion efficiency is assumed to be almost equal in all wave conditions (but see, Ref.[37]). The spectral power is known from the wave conditions and device efficiency under constrained wave-by-wave control can be estimated for a particular device. Thus, the converted power is,

$$P_c(\tau) = P_s(\tau)\ell, \tag{12}$$

where $P_s = 0.49 H_s^2 T_e D$ is the spectral wave power incident over a diameter D of an axisymmetric device, and ℓ is the overall power conversion efficiency.

$$R(\tau) = UP_c = U\left(P_m + \Delta P_1 + \Delta P_2 + \ldots\right)\ell, \tag{13}$$

where $\Delta P_n = P_n - P_m$, for the $N = 4$ relevant spectral variation periods here. The only variable that can be varied for a given deployment site and a given device type is thus U, the number of device units deployed. Optimizing an increasing $R(\tau)$ therefore amounts to determining the rate at which new device units need to be added. It is recalled that favorable or unfavorable interactions among device units are not considered here. Since ΔP_n are an order of magnitude smaller than P_m for the present site, the procedure adopted here consists of using $R_0(\tau) = U(\tau)P_m$, and optimizing

the function $R_0(\tau)$, here determined so that it best matches $G(\tau)$. The net $R(\tau)$ is then found using equation (13). Results (Section III) suggest that such an approach may be adequate in the present context. An action functional Ψ_R is now defined such that,

$$\Psi_R = \int_{T_0}^{T_R} \left[(R_0(\tau) - G(\tau))^2 + (T_R - T_0)^2 \left(\dot{R}_0(\tau) - \dot{G}(\tau) \right)^2 \right] d\tau. \tag{14}$$

Following the same reasoning as used for optimizing $G(\tau)$,

$$\frac{\partial \mathscr{L}}{\partial R_0} - \frac{d}{d\tau} \left(\frac{\partial \mathscr{L}}{\partial \dot{R}_0} \right) = 0. \tag{15}$$

so that,

$$\frac{d^2 R_0}{d\tau^2} - \frac{R_0}{(\tau_R - \tau_0)^2} = \frac{d^2 G}{d\tau^2} - \frac{G}{(\tau_R - \tau_0)^2}. \tag{16}$$

With $R_0(\tau) = U(\tau) P_m$, this condition leads to ($\tau_0 = 0$),

$$U(\tau) = \frac{G_R}{P_m} \left[1 - \cosh\left(\frac{\tau}{\tau_R} \right) + \coth 1 \sinh\left(\frac{\tau}{\tau_R} \right) \right]. \tag{17}$$

The optimum unit deployment function $U(\tau)$ is of course, here approximated by the nearest integer value at each τ. Then,

$$R(\tau) = U(\tau) \left(P_m + \Delta P_1 + \Delta P_2 + \Delta P_3 + \ldots \right). \tag{18}$$

kWH energy for estimating # houses or equivalent uses that can be powered can be found by integrating $R(\tau)$ over τ.

B. Minimum Time Deployment

Resilience is here interpreted in terms of being able to deploy over minimum time a specified capacity to meet demand. It is realized that a more compact variational strategy may result if one could begin by likening the recovery problem to the classic 'brachistochrone problem' of Variational Calculus[43]. With the rate at which more users are connected $G(\tau)$ on the horizontal axis, the rate at which more wave energy conversion capacity is added forms the ordinate. At a desired 'acceleration' a in the direction of increasing $R(\tau)$, the goal here is find a trajectory in the $G-R$ plane that minimizes the time taken by $R(\tau)$ to increase from $G = 0$ to G_R. For a trajectory $s(\tau)$ in the $G-R$ plane,

$$\frac{ds}{d\tau} = \sqrt{2aR}. \tag{19}$$

It follows from,

$$ds = \sqrt{dG^2 + dR^2} = \left[1 + \left(\frac{dR}{dG}\right)^2\right]^{1/2} dG, \tag{20}$$

that,

$$d\tau = \left[\frac{1 + R'^2}{2aR}\right]^{1/2} dG. \tag{21}$$

The total time the trajectory takes for moving R from $G = 0$ to $G = G_R$ is,

$$\tau = \int_0^{G_R} \left[\frac{1 + R'^2}{2aR}\right]^{1/2} dG \tag{22}$$

Denoting the integrand as $\mathscr{L}(R, R')$, for a stationary value of τ, $\delta\tau = 0$, and,

$$\frac{\partial \mathscr{L}}{\partial R} - \frac{d}{d\tau}\left(\frac{\partial \mathscr{L}}{\partial R'}\right) = 0, \;\; R(0) = 0;\; R(\tau) = G_R. \tag{23}$$

It is useful here to invoke the fact that $\mathscr{L}$ has no explicit dependence on τ, so that, equation (23) implies[44],

$$\mathscr{L} - R' \frac{\partial \mathscr{L}}{\partial R'} = C, \tag{24}$$

Letting $C_m = 1/2aC^2$, some algebra leads to,

$$G(\varphi) = \frac{C_m}{2}(2\varphi - \sin\varphi); \;\; R(\varphi) = \frac{C_m}{2}(1 - \cos\varphi). \tag{25}$$

The trajectory represented by equation (25) is a cycloid. C_m is related to the desired power generation at τ. φ goes from 0 to φ_R, where $\varphi_R = 1.2$, chosen such that $G(\varphi_R) = R(\varphi_R)$. Then, carrying the integration through in equation (22),

$$\tau_R = \varphi_R \sqrt{\frac{2C_m}{a}}, \tag{26}$$

for the chosen φ_R. As before, R here is replaced by $R_0 = UP_m$, where U is the number of device units deployed. As in Section II A, favorable or unfavorable interaction effects among device units are not considered here. Once $U(\varphi)$ is determined according to equation (25),

$$R(\varphi) = U(\varphi)(P_m + \Delta P_1 + \Delta P_2 + \ldots + \Delta P_N); \;\; N = 4. \tag{27}$$

kWH energy for estimating # houses or equivalent uses that can be powered can be found by integrating $R(\tau)$ over τ.

III. CALCULATIONS AND RESULTS

Calculations were carried out using wave statistics off Rincon, Puerto Rico, for November 2016, as reported by the CDIP 181 wave measurement buoy[36]. A 2-body axisymmetric system based on a cylindrical buoy and a submerged disc (with relative heave oscillations being used for energy conversion) was used (Figure 3), with $R = 8$m. For the average wave conditions for November 2016, the wave elevation time series were based on a 2-parameter Pierson-Moskowitz type wave spectral representation, as shown below. The spectral density was represented as,

$$S(\omega) = \frac{131.5H_s^2}{T_e^4\omega^5}\exp\left[-\frac{1054}{(T_e\omega)^4}\right]. \tag{28}$$

The wave elevation at a point x_A up-wave of the device was found using,

$$\eta(x_A;t) = \sum_{n=1}^{N} \Re\left\{A(\omega_n)\exp\left[-i\left(k(\omega_n)x_A - \omega_n t + \theta_n\right)\right]\right\}, \tag{29}$$

where,

$$A(\omega_n) = \sqrt{2S(\omega_n)\Delta\omega}, \tag{30}$$

and θ_n is a random number $\in [0, 2\pi]$; with $S(\omega_n)$ representing the spectral density value at ω_n. The wave elevation at the model location x_B was predicted at a time $t_p = 30$s into the future, using the expression,

$$\eta(x_B;t) = \int_{-\infty}^{\infty} h_l(\tau)\eta(x_A;t-\tau)d\tau, \tag{31}$$

where h_l is the impulse-response function representing the propagation kinematics, and is found as discussed in previously reported work[26].

Whereas the formulation in section (II) is described in terms of a single-mode device, the device used in the present work is a 2-body device, for which the equations of motion for heave oscillation of the two bodies can be reduced to a single equation for the relative heave oscillation[26,39] (as summarized in the Appendix). The hydrodynamic coefficients used for the two bodies are derived using published data[18]. Actuation is electro-hydraulic (potentially single or multiple cylinders[37]). The effect of mooring cables on the device stiffness is ignored. As in[26], the average converted power in the time domain is found using,

$$P_c = \frac{1}{T}\int_0^T F_{cr}(t)u_o(t)dt,$$

where $T = 1200$s was used. u_o denotes the optimum velocity under constraints. With the mean converted power value determined as above, the two optimization strategies are tested using a Matlab code. Results are presented in Figures 5–7 for the maximum recovery strategy, and in Figures 8–11 for the minimum-time strategy. Results are discussed in the following section.

IV. DISCUSSION OF RESULTS

As indicated earlier, wave conditions may vary significantly over the period of deployment. While wave profiles vary over time scales of 1-20s, wave statistics (i.e. statistical parameters such as mean wave height, significant wave height, mean wave period, energy period, etc.) may remain approximately constant over time scales such as 20-30 minutes. An example of power spectral density variation over a month is shown in Figure 1, for a measurement location off Rincon, Puerto Rico for the month of November, 2016, with the period in hours shown on the x-axis. The power spectrum is seen to vary considerably over this period, and the largest peak represents the monthly mean conditions of $H_{sm} = 1.4$m, $T_{em} = 9.4$s. Smaller variations about the monthly mean are shown in Figure 2 with frequency in 1/hour on the x-axis. For a proposed deployment period of 5-7 days, it is noted that only the variation-peaks up to 90 hours seem relevant. The shortest-period significant peak in this range has a period of 13 hours, with the longest-period included in the calculations being 90 hours (Figure 2). In each case, the spectral density variations relative to the mean are seen to be about an order of magnitude smaller than the power conversion under the monthly mean conditions.

An example of short-term variation in power conversion under wave-by-wave impedance matching with displacement constraint for the monthly mean wave conditions is shown in Figure 4. The mean power converted over 20 minutes is also shown in Figure 4. It is recalled that the results in Figure 4 are for an omni-directional axisymmetric heaving buoy device with a shallowly-submerged reaction plate (the buoy radius being $R = 8$m). These results are representative of the expected power conversion performance for the chosen device for the monthly average conditions. Small changes in wave conditions will cause small changes in the mean converted power, even when the conversion performance is at its practically attainable constrained optimal. However, the approach taken in the present work is to optimize the deployment strategy with respect to the monthly mean wave statistics, and over the optimal trajectories to superimpose the effect of the smaller variations in wave statistics. It is anticipated that the overall deployment strategy will

still be close to optimal in terms of power conversion performance if monthly mean statistics and wave-statistic variations for the same month from the previous two years (for instance) are used to assist on-site planning. It is also worth keeping in mind that the strategies evaluated here are to be provided as an input to recovery planners, and practical considerations could force additional changes to the optimum deployment trajectories.

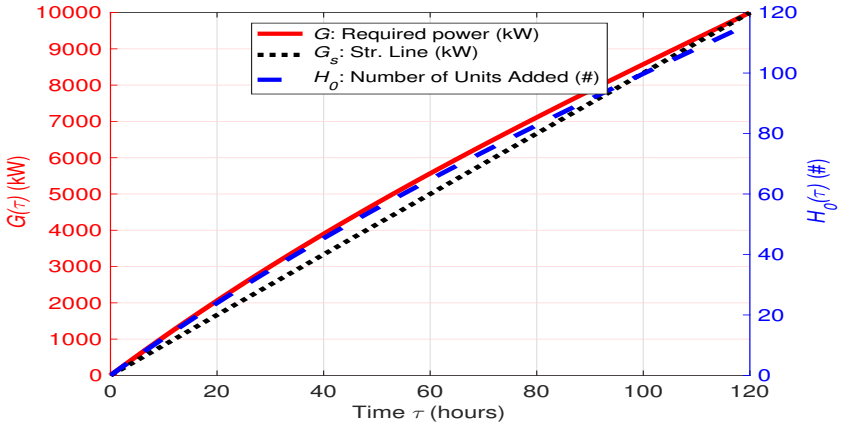

FIG. 5. Strategy 1: maximum capacity recovery in prescribed time. The figure show the number of units to be added over 5 days to maximize capacity.

Figures 5 to 7 plot the results for the maximum recovery strategy, whereas the results for the minimum-time recovery strategy are shown in Figures 8 to 11. It should be noted that for the maximum power recovery strategy, the function G also includes any necessary storage planned as part of the recovery process. The recovery curve in Figure 5 is a hyperbolic sine form [equations (10) and (17)]. The left hand y-axis on the plot in Figure 5 shows the amount of power demand restored using wave energy converters alone, regardless of its intended use. The short-dashed line shows power-conversion recovery along a straight line from $G(0) = 0$ to the desired $G(\tau_R) = G_R = 10$ MW. Compared with a straight line, the optimal trajectory as determined here is found to provide greater recovery for the same recovery time. The long-dashed line plots the number of device units to be deployed and connected in order to meet the increasing power demand. The time axis is in hours, indicating that in order to provide 10 MW over 5 days, about 120 units will need to be connected.

It is recalled that omni-directional 2-body heaving axisymmetric devices are used here for their independence from the need for sea-floor based reference inertias. Although better conversion efficiencies (and greater power per unit) are available with deeply submerged reaction masses[39], the

relatively shallowly submerged reaction mass in the present work could make for easier transportation and deployment. However, the feasibility of an operation aimed at transporting and deploying the required number of units (for generating the desired power amounts) needs to be considered further.

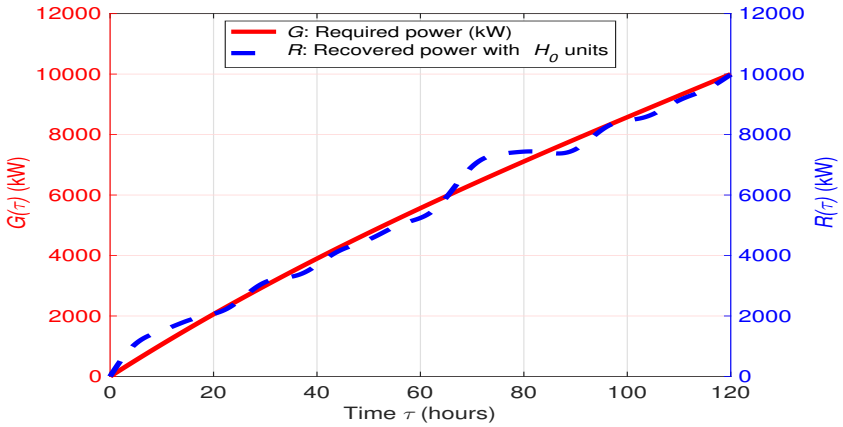

FIG. 6. Strategy 1: maximum capacity recovery in prescribed time. The figure plots the effect of variability in wave statistics about the monthly mean. Mean converted power is shown.

Figure 6 shows the effect of wave-statistic variations on the power supplied by the wave energy device units. For the most part, for the present site, the power supplied is seen to be slightly smaller or somewhat greater than the power needed on the optimum recovery trajectory.

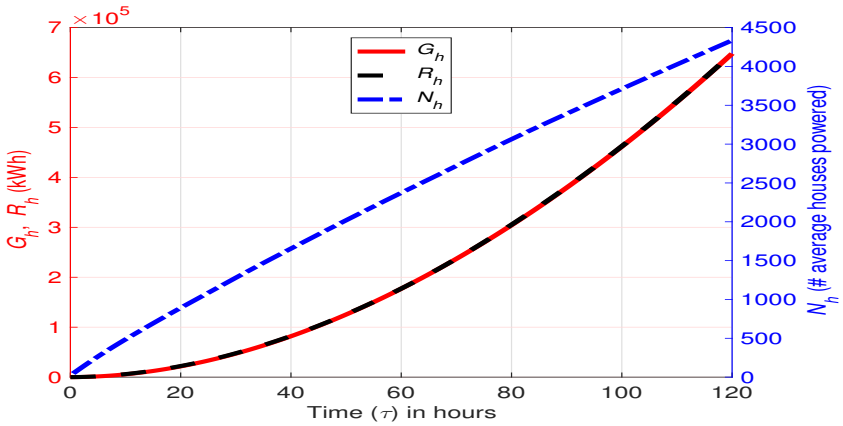

FIG. 7. Strategy 1: maximum capacity recovery in prescribed time. Number of houses connected over 5 days (897 kWh per house, based on EIA 2017 figures[45] is used for perspective; equivalent power could be used for other purposes instead.

Figure 7 plots the supplied and generated energy in kWH units as indicated on the left-hand y-axis, while the equivalent result in terms of number of houses reconnected is shown on the right-hand y-axis. It should be pointed out that the effect of the spectral statistic variations is included in the kWH generated capacity calculations, and is found to have been largely 'integrated out' of the recovery process over 5 days. The number of houses connected is used as an example in this work, whereas the energy could instead (or in addition) also be directed for other recovery applications such as desalination, deflooding, and construction.

Figure 8 plots the converted power as a function of required power for minimizing the time taken for recovery. The different traces in the plot are for different values of the 'recovery rate parameter' a. For the type of power amounts and recovery times being considered here, a recovery-rate parameter value $a = 6$ is chosen as adequate. However, studies with other values of a could provide further insights.

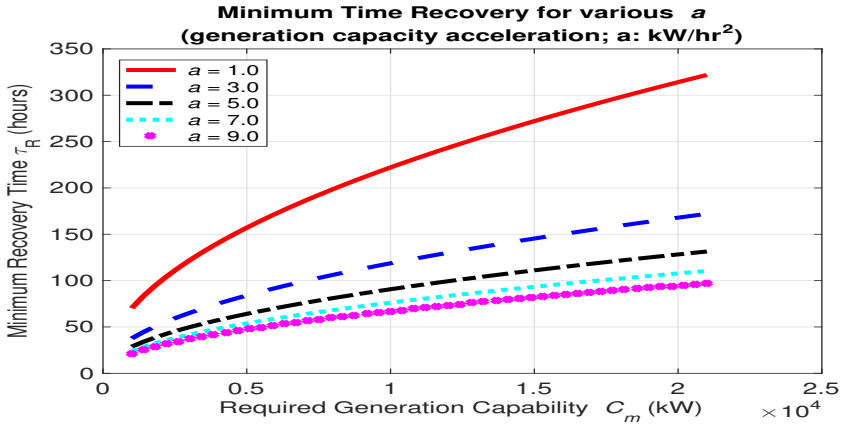

FIG. 8. Strategy 2: minimum time for specified power capacity recovered. Plot comparing different values of the recovery-rate parameter a. $a = 6$ was chosen in this work.

Figure 9 plots the supplied power as a function of time in hours on the left-hand y-axis, which also indicates the power converted. The dash-dot line shows the converted power trajectory. The required capacity of 10 MW is seen to be recovered in 80 hours. As the short-dashed line indicates, straight-line recovery provides better conversion for the first 45 hours for the present target of 10 MW. However, the minimum-time optimum trajectory provides better conversion beyond that point, reaching 10 MW in 80 days, while the straight-line trajectory reaches that level over 120 days. The converted power results translate directly to the number of units required, shown on the right-hand y-axis. The number of units to be deployed to provide 10 MW is found be

419 approximately the same as with the maximum-recovery strategy.

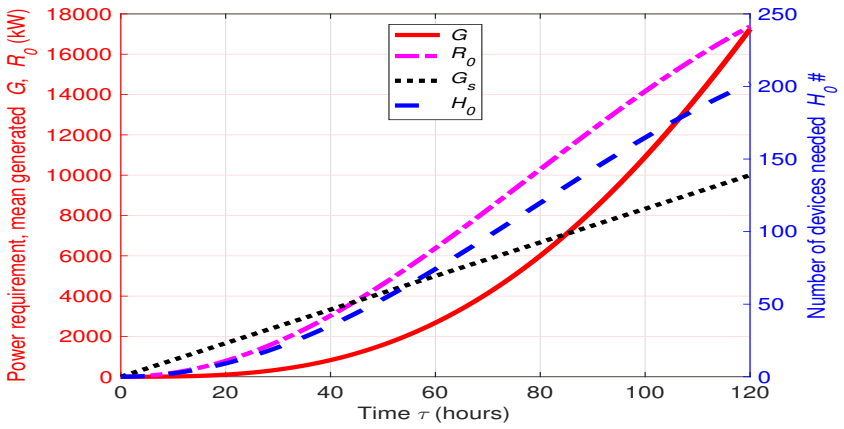

FIG. 9. Strategy 2: minimum time for specified power capacity recovered. The figure shows the number of units to be added.

420 The effect of wave-statistic variations is shown in Figure 10. Since the converted power exceeds
421 the supplied power through during the 80-hour period (for reaching 10 MW), small changes caused
422 by variations in the spectral statistics are potentially less limiting for this strategy. Figures 9 and
423 10 suggest that storage need not be included explicitly in the function G for this strategy, but that
424 it should result as a by-product of the minimum-time strategy.

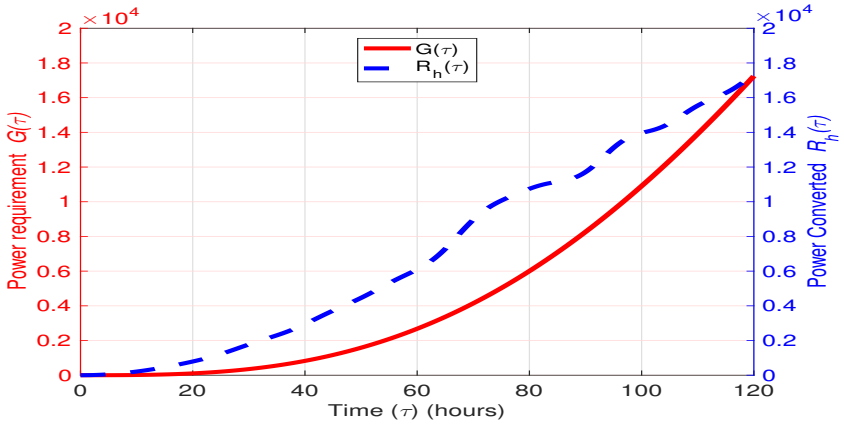

FIG. 10. Strategy 2: minimum time for specified power capacity recovered. The figure plots the effect of wave statistics variability on mean converted power.

425 Figure 11 plots the results in integrated, energy units, where the left-hand y-axis plots the
426 energy supply recovered, while the right-hand y-axis shows the energy amount converted in terms

of the number of houses connected. This number is seen to be comparable to that seen with the maximum recovery strategy. Once again, it is noted that other energy uses such as desalination, deflooding, etc. are also possible to address within the present framework.

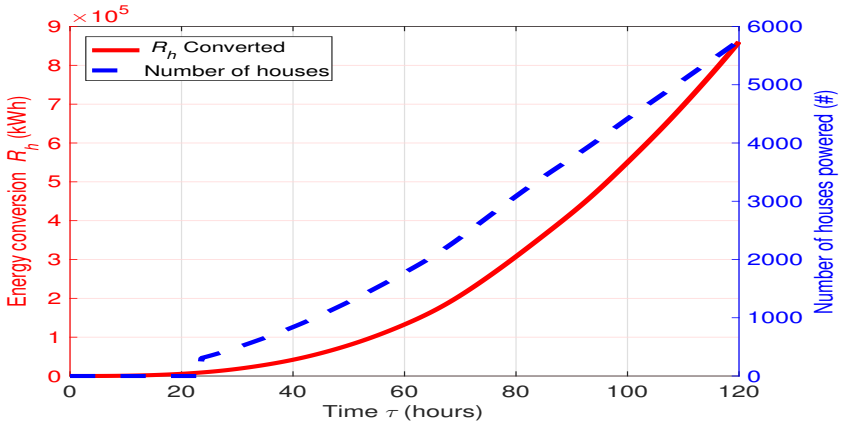

FIG. 11. Number of houses connected over 5 days (897 kWh per house; EIA 2017 figures approximated). # houses used for perspective; equivalent power could be used for other purposes instead.

Tables I and II summarize the overall findings for the two strategies for different power-level objectives. The more significant differences for small and intermediate power levels between the maximum recovery and minimum time strategies perhaps can be attributed to the particular choice of the parameter a in this work. The current value, $a = 6$, leads to an optimum use of the devices when the desired power goal is 10MW (recovered over 80 days), and a different value may be preferable for smaller power amounts. The differences in the number of houses powered (related to kWH available for any desired use) is due to the form of the power curves and the number of hours for recovery for the two strategies (maximum recovery over prescribed time strategy and minimum time strategy).

TABLE I. Strategy 1:maximum recovery over a prescribed time period; range of expectations.

Power (MW)	# Units Needed	# Houses Powered	Hours
2.0	23	870	120
5.0	58	2160	120
10.0	118	4300	120

TABLE II. Strategy 2: minimum time recovery for prescribed power capacity: range of expectations.

Power (MW)	# Units Needed	# Houses Powered	Hours
2.0	25	400	50
5.0	70	1200	70
10.0	121	3200	80

Future work on this effort could be based on the following considerations. Overall, it appears that modest power supply and power conversion requirements could be met using 2-body axisymmetric wave energy devices, even though the number of units required for doing so needs to be considered further. Specifically, because the present device is being controlled for constrained optimal (impedance matching) control on a wave-by-wave basis, its performance can be said to be at a level close to the best available. For this reason, the situation seems to demand devices with more efficient hydrodynamics that are still easily transportable by sea. Ideally, the type of power targets desired here should require about a tenth of the number of units currently necessary, without an excessive increase in device size (since a device 8m in radius can already be considered large). Finally, favorable or unfavorable array effects due to interactions between units are not considered in this work. Avoidance of interactions could require that the number of units per available deployment area be accounted for via constraints to be adjoined with the current Lagrangians in Sections II A and II B. In addition, the effect of possible wave nonlinearity in the near-shore deployment regions also needs to be accounted for, by providing an estimate on the uncertainty in the converted power estimates discussed earlier in this section.

V. CONCLUSIONS

It can be argued that the lower energy densities of renewable energy sources (such as wave energy) tend to work favorably from a resilience and recovery standpoint. A large number of renewable energy converter units distributed over a sizeable area would typically be required for meeting prescribed energy demands. It is plausible that, whereas severe local damage due to extreme events could disrupt the operation of an entire generation plant based on high-density fuels, such damage might only incapacitate a smaller proportion of the generation facility in the case of low-density renewable sources. In addition, in the case of wave energy converters, recovery

operations could be better targeted through selective deployment close to affected areas, where additional units could be transported to location by sea, i.e. without requiring major land-based operations.

Considerable further work is needed, however, in order to improve the energy conversion technology itself in terms of its power capture, structural, transportation, and deployment efficiencies. Thus, while wave energy devices typically are designed for long-term operation at particular sites, in an application such as proposed here, they would need to be designed to operate efficiently and safely at a number of different sites. The proposed application may thus provide some design and optimization challenges that should prove to be of interest.

The present results indicate that there may be scope, concurrently to optimize device sizes with number of units to be deployed, taking into account conversion efficiencies and ease of transportation and deployment. It is interesting to note that, close to damaged sites, the waters may be relatively shallow, in which case, shallow-draft devices may be preferable. It is likely therefore that one large floating transportable structure housing a number of smaller converters within it (such as the *Kaimei* vessel) could be worth considering in the short run, if hydrodynamic control for high efficiency operation could be used. Also in the near term, wave energy converters may prove useful as a potentially attractive option in isolated and fragile grids facing black-start situations. In addition to use in potential black-start operations, it would be interesting to consider using progressively deployed wave energy devices directly to assist in short-term recovery operations. Short term recovery would typically involve (in addition to grid black start) augmenting emergency generation facilities for hospitals, essential businesses, street repair, street/traffic lighting, refrigeration, water treatment, air-traffic control, local communication systems[46], etc. (Figure 12,[46]). It is expected that, as more of the original generation and power grid capability is recovered, the wave energy device units would be transported to a different location to facilitate different recovery operations. Additional use of progressively deployed wave energy devices to provide desalinated drinking water and to power operations such as deflooding may also be worth considering. It is recognized, however, that the magnitude of recovery operations may in several instances may be too large for one particular power source, and additional use of solar, wind, marine tidal current and hydroelectric (where possible) energy may become necessary; and should be considered within an overall optimization study.

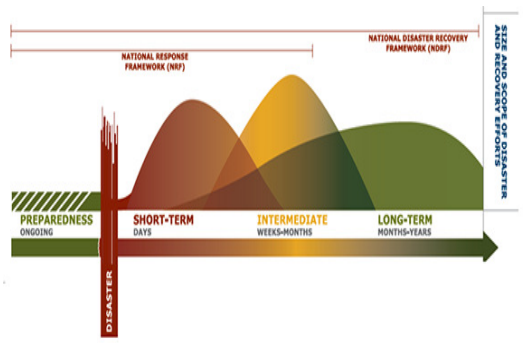

FIG. 12. Recovery continuum as understood by the U.S. Federal Emergency Management Agency (FEMA)[46]. The present technique could participate in short-term recovery operations. Reproduced by permission from the U.S. Federal Emergency Management Agency (April, 2019).

ACKNOWLEDGMENTS

It is a pleasure to thank Professor Ben Hobbs for the numerous discussions on resilience, energy sustainability, and optimization techniques. Much gratitude is due to Dr. John Kamp at the Defense Advanced Research Projects Agency and Mr. William McShane at the Department of Energy for their continuing and helpful feedback on this work.

REFERENCES

[1]USGCRP-I, "Climate Science Special Report: Fourth National Climate Assessment, Volume I," Tech. Rep. (U.S. Global Change Research Program, Washington, DC, USA, 2017).

[2]USGCRP-II, "Impacts, Risks, and Adaptation in the United States: Fourth National Climate Assessment, Volume II," Tech. Rep. (U.S. Global Change Research Program, Washington, DC, USA, 2018).

[3]NWS, "Major Hurricane *Maria* - September 20, 2017," The National Weather Service (2017), https://www.weather.gov/sju/maria2017.

[4]L. Lazo, "*Michael* cleanup in Florida panhandle hampered by damaged roads, power outages," *The Washington Post* (2018).

[5]DOE, "Potential Maritime Markets for Marine and Hydrokinetic Technologies:Draft Report," Tech. Rep. (Department of Energy: Office of Energy Efficiency and Renewable Energy, Washington, DC, USA, 2018).

[6]S. H. Salter, "Wave power," Nature , 720–724 (1974).

[7]E. Lewis, *Principles of Naval Architecture*, Vol. II (Society of Naval Architects and Marine Engineers, NJ, 1988) Chap. 4.

[8]A. F. O. Falcão, "Wave energy utilization: a review of the technologies," Renewable and Sustainable Energy Reviews **14**, 899–918 (2010).

[9]S. H. Salter, "Recent progress on ducks," in *Proc. 1st Symposium on Wave Energy Utilization, Gothenburg, Sweden* (1979).

[10]S. H. Salter, "Progress on Edinburgh ducks," in *Proc. IUTAM Symp. Hydrodynamics of Wave Energy Utilization*, edited by D. Evans and A. de O. Falcão (Springer Verlag, Berlin, 1985) pp. 35–50.

[11]K. Budal and J. Falnes, "Optimum operation of improved wave power converter," Marine Science Communication **3**, 133–150 (1977).

[12]D. V. Evans, D. C. Jeffrey, S. H. Salter, and J. R. M. Taylor, "Submerged cylinder wave energy device: theory and experiment," Applied Ocean Research **1**, 3–12 (1979).

[13]Y. Masuda, "Experimental full-scale results of wave power machine Kaimei in 1978," in *Proc. 1st International Symposium on Wave Energy Utilization, Gothenburg, Sweden* (1979) pp. 349–360.

[14]R. Yemm, D. Pizer, C. Retzler, and R. Henderson, "Pelamis: experience from concept to connection," Philosophical Transactions of the Royal Society A, Mathematical, Physical, and Engineering Sciences **370**, 365–380 (2012).

[15]E. Friis-Madsen, H. C. Sorensen, and S. Parmeggiani, "The development of a wave dragon 1.5 MW demonstrator," in *Proc. 4th International Conference on Ocean Energy* (2012) october, 2012, Dublin.

[16]E. Mehlum and J. J. Stammes, "Power production based on focusing ocean swells," in *Proc. 1st Symposium on Wave Energy Utilization, Gothenburg, Sweden* (1979) pp. 29–35.

[17]B. M. Count, "Wave power – a problem searching for a solution," in *Power from Sea Waves*, edited by B. Count (Academic Press, London, 1980) pp. 11–27.

[18]H. Eidsmoen, *On the theory and simulation of heaving-buoy wave-energy converters with control*, Ph.D. thesis, Norwegian University of Science and Technology (1995), Trondheim, Norway.

[19]S. H. Salter, "Development of the duck concept," in *Proc. Wave Energy Conference* (1978) Heathrow, U.K.

[20]K. Budal and J. Falnes, "Interacting point absorbers with controlled motion," in *Power from Sea Waves*, edited by B. M. Count (Academic Press, London, 1980) pp. 381–399.

[21]P. Nebel, "Maximizing the efficiency of wave-energy plants using complex conjugate control," Proc. IMechE Part I - Journal of Systems and Control Engineering **206**, 225–236 (1992).

[22]D. Skyner, "Solo duck linear analysis," Tech. Rep. (University of Edinburgh, 1987).

[23]R. H. Hansen and M. M. Kramer, "Modeling and control of the wave star prototype," in *Proc. 9th European Wave and Tidal Energy Conference* (2011) southampton, UK, paper 163.

[24]S. Naito and S. Nakamura, "Wave energy absorption in irregular waves by feedforward control system," in *Proc. IUTAM Symp. Hydrodynamics of Wave Energy Utilization*, edited by D. Evans and A. de O. Falcão (Springer Verlag, Berlin, 1985) pp. 269–280.

[25]J. Falnes, "On non-causal impulse response functions related to propagating water waves," Applied Ocean Research **17**, 379–389 (1995).

[26]U. A. Korde, "Near-optimal control of a wave energy device using deterministic-model driven incident wave prediction," Applied Ocean Research **53**, 31–45 (2015).

[27]M. S. Longuet-Higgins, "The statistical analysis of a random moving surface," Philosophical Transactions of the Royal Society of London, Series A **249**, 321–387 (1957).

[28]J. W. Feltes and C. Grande-Moran, "Black start studies on system restoration," in *Proc. IEEE Power and Energy Society General Meeting* (2008) p. 8p.

[29]J. R. Minkel, "The 2003 northeast blackout: Five years latter," Scientific American (2008).

[30]P. Danjcek, "Mass-power outage in disasters: addressing inefficiencies in FEMA's generator mission," Tech. Rep. (Johns Hopkins University, Baltimore, MD, USA, 2014).

[31]J. A. Lopes, C. L. Decas, and F. O. Resende, "Microgrids black start and islanded operation," in *Proc. 15th PSCC* (Liege, Belgium, 2005).

[32]A. Colthorpe, "California battery's black start capability hailed as major accomplishment," Energy Industry (2017).

[33]IEC, "Key world energy statistics: Microgrids for disaster preparedness and recovery," Tech. Rep. (International Electrotechnical Society, Sweden, 2014).

[34]ORDOE, "Distributed Energy Resilience Study," Tech. Rep. (Oregon Department of Energy, 2011) prepared by R.W. Beck.

[35]M. Bruneau, S. E. Chang, R. T. Eguchi, G. C. Lee, T. D. O'Rourke, A. M. Reinhern, and M. Shinozuka, "A framework to quantitatively assess and enhance the seismic resilience of communities," Earthquake Spectra **19**, 733–752 (2003).

[36]CDIP, "Wave measurements at CDIP 181," (2019), coastal Data Information Program, Scripps Institution of Oceanography, University of California, SD; http://cdip.ucsd.edu/.

[37]U. A. Korde and J. B. Richon, "Recent experimental testing of a 2-body wave energy converter under wave-by-wave impedance matching control," (2018), technical report to the National Science Foundation, U.S.

[38]D. V. Evans, "Power from water waves," Annual Review of Fluid Mechanics **13**, 157–187 (1981).

[39]J. Falnes, "Wave-energy conversion through relative motion between two single-mode oscillating bodies," J Offshore Mechanics and Arctic Engineering-Transactions of the ASME **121**, 32–36 (1999).

[40]U. A. Korde, "Wave energy conversion under constrained wave-by-wave impedance matching with amplitude and phase-match limits," (2019), preprint.

[41]W. Cummins, "The impulse response function and ship motions," Tech. Rep. (David Taylor Model Basin DTNSRDC, 1962).

[42]U. A. Korde and J. V. Ringwood, *Hydrodynamic Control of Wave Energy Devices* (Cambridge University Press, Cambridge, UK, 2016) Chap. 4.

[43]C. Lanczos, *The Variational Principles of Mechanics* (University of Toronto Press, CA, 1970) reissued by Dover Inc, NY, 1986.

[44]R. Weinstock, *Calculus of Variations: with applications to Physics and Engineering* (Dover, NY, 1974) 1974 reissue of the 1952 McGraw-Hill edition.

[45]EIA, "How much energy does an American household use," Tech. Rep. (Energy Information Agency, Washington, DC, USA, 2017).

[46]FEMA, "National Disaster Recovery Framework," Tech. Rep. (Federal Emergency Management Agency, Washington, DC, USA, 2016).

[47]U. A. Korde, J. J. Song, R. D. Robinett, and O. Abdelkhalik, "Hydrodynamic considerations in near-optimal control of a wave energy converter for ocean measurement applications," Marine Technology Society Journal **51**, 44–57 (2017).

APPENDIX

As described in previous work[26] and[47], the frequency domain model for the present 2-body device can be written as

$$\begin{aligned}
&[Z_t(i\omega)+Z_L(i\omega)]\,v_t(i\omega)+i\omega\,[Z_c(i\omega)-Z_L(i\omega)]\,v_b(i\omega)=F_{ft}(i\omega)\\
&[Z_c(i\omega)-Z_L(i\omega)]\,v_t(i\omega)+[Z_b(i\omega)+Z_L(i\omega)]\,v_b(i\omega)=F_{fb}(i\omega)
\end{aligned} \tag{32}$$

where the matrix elements are defined as,

$$\begin{aligned}
Z_t(i\omega)&=i\omega\,[m_t+\overline{a}_t(\infty)+a_t(\omega)]+\frac{k_t}{i\omega}+(c_{dt}+b_{dt}(\omega))\\
Z_b(i\omega)&=i\omega\,[m_b+\overline{a}_b(\infty)+a_b(\omega)]+\frac{k_b}{i\omega}+(c_{db}+b_{db}(\omega))\\
Z_c(i\omega)&=i\omega a_c(\omega)+b_c(\omega)\\
Z_L(i\omega)&=L(\omega)+\frac{N(\omega)}{i\omega}
\end{aligned} \tag{33}$$

Where the letter m is used to denote in-air mass with the subscripts t and b respectively denoting the top and bottom bodies. b_{dt} and b_{db} denote the frequency-dependent radiation damping for the two bodies, while $\overline{a}_t(\infty)$ and $\overline{a}_b(\infty)$ denote the infinite-frequency added masses for the two bodies and $a_t(\omega)$ and $a_b(\omega)$ represent just the frequency-dependent parts of the respective added masses. The letter k denotes stiffness (hydrostatic for the floating buoy and mooring-related for the submerged disc), while c_{dt} and c_{db} represent the linearized viscous damping coefficients. a_c and b_c denote the frequency-variable added mass and radiation damping due to coupling between the two bodies. Z_L represents the load impedance applied by the power take-off on the relative oscillation. Following the approach of Falnes[39], it is possible to express equation (32) as a scalar equation in terms of the relative velocity $v_r(i\omega)$,

$$v_r(i\omega)=v_t(i\omega)-v_b(i\omega), \tag{34}$$

by defining,

$$\overline{Z}(i\omega)=Z_t(i\omega)+Z_b(i\omega)+2Z_c(i\omega), \tag{35}$$

and

$$F_f(i\omega)=\frac{F_{ft}(i\omega)\,(Z_b(i\omega)+Z_c(i\omega))}{\overline{Z}(i\omega)}-\frac{F_{fb}(i\omega)\,(Z_t(i\omega)+Z_c(i\omega))}{\overline{Z}(i\omega)}. \tag{36}$$

it is seen that

$$v_r(i\omega)=\frac{F_f(i\omega)}{Z_i(i\omega)+Z_L(i\omega)}, \tag{37}$$

where

$$Z_i(i\omega) = \frac{Z(i\omega)Z_s(i\omega) - Z_c^2(i\omega)}{\overline{Z}(i\omega)}. \tag{38}$$

In the analysis of Section II,

$$\begin{aligned} U(i\omega) &\leftarrow v_r(i\omega), \\ b(\omega) &\leftarrow \Re\left(Z_i(i\omega)\right), \\ C(\omega) &\leftarrow \Im\left(Z_i(i\omega)\right). \end{aligned} \tag{39}$$

With,

$$\begin{aligned} u(t) &= \frac{1}{2\pi}\int_{-\infty}^{\infty} U(i\omega)\mathrm{e}^{i\omega t}d\omega, \\ h_b(t) &= \frac{1}{2\pi}\int_{-\infty}^{\infty} b(\omega)\mathrm{e}^{i\omega t}d\omega, \\ h_a(t) &= \frac{1}{2\pi}\int_{-\infty}^{\infty} C(\omega)\mathrm{e}^{i\omega t}d\omega. \end{aligned} \tag{40}$$

Further,

$$\begin{aligned} h_r(t) &= h_b(t) + h_a(t), \\ h_c(t) &= h_b(t) - h_a(t). \end{aligned} \tag{41}$$

$h_b(t)$ is an even function, and $h_a(t)$ is an odd function, so that $h_r(t)$ is causal, and $h_c(t)$ is anticausal. Since, $h_r(t) \to 0$, $t \to t_r$, where t_r is typically 20-30 seconds, It is easier in practice to use $h_b(t)$ and $h_a(t)$ separately, with velocity predictions, which in turn are based on wave elevation predictions. Further details, including the need to predict the exciting force, are discussed in Ref.[42].